SCIENTIFIC REPORTS
nature research

OPEN

Advanced Glycation End-Products Suppress Mitochondrial Function and Proliferative Capacity of Achilles Tendon-Derived Fibroblasts

Received: 27 February 2019
Accepted: 16 August 2019
Published online: 30 August 2019

Shivam H. Patel[1], Feng Yue[2], Shannon K. Saw[1], Rachel Foguth[3,4], Jason R. Cannon[3,4], Jonathan H. Shannahan[3], Shihuan Kuang[2], Arman Sabbaghi[5] & Chad C. Carroll[1,6]

Debilitating cases of tendon pain and degeneration affect the majority of diabetic individuals. The high rate of tendon degeneration persists even when glucose levels are well controlled, suggesting that other mechanisms may drive tendon degeneration in diabetic patients. The purpose of this study was to investigate the impact of advanced glycation end-products on tendon fibroblasts to further our mechanistic understanding of the development and progression of diabetic tendinopathy. We proposed that advanced glycation end-products would induce limitations to mitochondrial function and proliferative capacity in tendon-derived fibroblasts, restricting their ability to maintain biosynthesis of tendon extracellular matrix. Using an *in-vitro* cell culture system, rat Achilles tendon fibroblasts were treated with glycolaldehyde-derived advanced glycation end-products (0, 50, 100, and 200 μg/ml) for 48 hours in normal glucose (5.5 mM) and high glucose (25 mM) conditions. We demonstrate that tendon fibroblasts treated with advanced glycation end-products display reduced ATP production, electron transport efficiency, and proliferative capacity. These impairments were coupled with alterations in mitochondrial DNA content and expression of genes associated with extracellular matrix remodeling, mitochondrial energy metabolism, and apoptosis. Our findings suggest that advanced glycation end-products disrupt tendon fibroblast homeostasis and may be involved in the development and progression of diabetic tendinopathy.

Over 30 million Americans suffer from diabetes. Evaluation of this patient population suggests that tendon abnormalities (i.e., tendinopathies) such as collagen fibril disorganization, increased tissue stiffness, and tissue degeneration are present in the majority of diabetic individuals[1–3]. Notably, the high rate of tendinopathies in diabetic individuals persists even when glucose levels are well controlled (hemoglobin A1c <7)[2,4,5]. Given the high prevalence of diabetic tendinopathy, there is a critical need to define the molecular process underlying the diabetic tendon phenotype.

Advanced glycation end-product (AGE) formation is a non-enzymatic process in which free amine terminals are subjected to covalent modification by reactive glucose or other carbonyl containing molecules. AGEs form at an accelerated rate in diabetes and these modifications can result in non-enzymatic cross-links in long-lived extracellular proteins such as tendon collagen, which increase tissue stiffness and alter tissue mechanical properties[6–10]. Furthermore, circulating AGE adducts are able to interact with the receptor for advanced glycation end-products (RAGE) to initiate a noxious feed forward cycle of sustained inflammation and tissue damage[11]. In other tissues, endogenous AGE formation as result of chronic hyperglycemia and spontaneous oxidation of glycolytic intermediates contribute significantly to elevated levels of bound and circulating AGE adducts in diabetic patients[12,13]. Additionally, AGE-rich diets can increase serum AGE levels and result in accumulation of AGEs in

[1]Department of Health and Kinesiology, Purdue University, West Lafayette, IN, USA. [2]Department of Animal Sciences, Purdue University, West Lafayette, IN, USA. [3]School of Health Sciences, Purdue University, West Lafayette, IN, USA. [4]Purdue Institute for Integrative Neuroscience, West Lafayette, IN, USA. [5]Department of Statistics, Purdue University, West Lafayette, IN, USA. [6]Indiana Center for Musculoskeletal Health, Indiana University School of Medicine, Indianapolis, IN, USA. Correspondence and requests for materials should be addressed to C.C.C. (email: carrol71@purdue.edu)

tendon of mice[14]. It is not known, however, what role circulating AGEs play in the development and progression of diabetic tendinopathy.

In non-tendon models, AGEs have been shown to activate RAGE-mediated cellular pathways leading to impairments in mitochondrial function and apoptosis[15–18]. To our knowledge, the impact of AGEs on tenocyte mitochondrial function (e.g., ATP production and electron transport efficiency) has not previously been evaluated. Specifically, ATP has been shown to promote biosynthesis of the extracellular matrix (ECM) in intervertebral cells[19]. In diabetic tendinopathy, degeneration and loss of organization in the ECM may be driven, in part, by the imbalance of energy (ATP) demand and supply. We propose that AGEs contribute to the diabetic tendon phenotype by activating cellular pathways that limit mitochondrial function, thereby interfering with the capacity of tendon fibroblasts to maintain biosynthesis of tendon ECM.

In effort to better understand diabetes associated tendon pathology, we sought to characterize impairments to energy producing systems and proliferative capacity of tendon-derived fibroblasts in response to AGE treatment and high glucose containing medium. We hypothesized that AGEs, *in-vitro*, would impair mitochondrial function and proliferative capacity, independent of glucose concentrations. Further, we hypothesized that AGEs and high glucose medium would reduce mitochondrial DNA (mtDNA) content and further contribute to limitations imposed to energy producing pathways in tendon fibroblasts. To advance our understanding of mitochondrial biogenesis and energy production during AGE exposure, analyses of mitochondrial apoptotic regulators, as well as regulators of mitochondrial energy metabolism were completed. This study provides new functional and descriptive perspective of the AGE insult on tendon fibroblast homeostasis.

Results

Proliferative capacity. Cell proliferation (EdU), cell counts, Mybl2 mRNA, Pcna mRNA, and cytostatic MTT were significantly reduced at AGE-50 μg/ml, AGE-100 μg/ml, and AGE-200 μg/ml compared to AGE-0 μg/ml ($p < 0.0125$, Fig. 1b–f, respectively). The HG condition had no effect on cell proliferation (EdU), cell counts, and Mybl2 mRNA ($p > 0.0125$, Fig. 1b–d, respectively). However, the HG condition reduced Pcna mRNA transcript counts ($p < 0.0125$, Fig. 1e) and increased absorbance values of cytostatic MTT data ($p < 0.0125$, Fig. 1f).

Mitochondrial stress tests. ATP production-coupled respiration was significantly reduced at AGE-100 μg/ml and AGE-200 μg/ml compared to AGE-0 μg/ml ($p < 0.0125$, Fig. 2a). ATP production-coupled respiration was also significantly reduced in the HG condition ($p < 0.0125$, Fig. 2a). Basal respiration was significantly reduced at AGE-100 μg/ml and AGE-200 μg/ml compared to AGE-0 μg/ml ($p < 0.0125$, Fig. 2b), but no glucose effect was observed ($p > 0.0125$, Fig. 2b). Neither AGE treatment nor glucose condition had a significant effect on maximal respiration ($p > 0.0125$, Fig. 2c). AGE treatment had no effect on proton leak ($p > 0.0125$, Fig. 2d), but the HG condition increased proton leak across the inner mitochondrial membrane ($p < 0.0125$, Fig. 2d). Coupling efficiency was significantly reduced at AGE-200 μg/ml compared to AGE-0 μg/ml ($p < 0.0125$, Fig. 2e). Coupling efficiency was also significantly reduced in the HG condition ($p < 0.0125$, Fig. 2e). Spare respiratory capacity was significantly increased at AGE-200 μg/ml compared to AGE-0 μg/ml ($p < 0.0125$, Fig. 2f), but no glucose effect was observed ($p > 0.0125$, Fig. 2f).

Mitochondrial membrane potential. AGE treatment had no effect on mitochondrial membrane potential ($p > 0.025$, Fig. 3), but mitochondrial membrane potential was decreased in the HG condition ($p < 0.025$, Fig. 3).

Transcriptional analysis of extracellular matrix remodeling. Col1a1 and MMP9 mRNA transcript counts were significantly reduced in the AGE-200 μg/ml compared to AGE-0 μg/ml ($p < 0.0125$, Fig. 4a,d). Col3a1 mRNA transcript counts were significantly increased in the AGE-50 μg/ml and AGE-100 μg/ml groups compared to AGE-0 μg/ml ($p < 0.0125$, Fig. 4b). MMP2 mRNA transcript counts were significantly increased in the AGE-100 μg/ml compared to AGE-0 μg/ml ($p < 0.0125$, Fig. 4c). AGEs had no effect on TIMP1 mRNA transcript counts ($p < 0.0125$, Fig. 4e). No glucose effect was observed for Col1a1, Col3a1, MMP2, MMP9, or TIMP1 ($0 < 0.0125$, Fig. 4a–e).

Mitochondrial DNA Content. mtDNA content was significantly increased at AGE-50 μg/ml, AGE-100 μg/ml, and AGE-200 μg/ml compared to AGE-0 μg/ml ($p < 0.0125$, Fig. 5a), but no effect of glucose condition was observed ($p > 0.0125$, Fig. 5a). Neither AGE treatment nor glucose condition had a significant effect on DNA content when normalized to cell counts ($p > 0.0125$, Fig. 5b).

Transcriptional Analysis of Mitochondrial Complexes. Ndufa1 mRNA transcript counts were significantly increased at AGE-50 μg/ml, AGE-100 μg/ml, and AGE-200 μg/ml compared to AGE-0 μg/ml ($p < 0.0125$, Fig. 6a), but no effect of glucose condition was observed ($p > 0.0125$, Fig. 6a). Sdha mRNA transcript counts were significantly reduced at AGE-200 μg/ml compared to AGE-0 μg/ml ($p < 0.0125$, Fig. 6b), but no effect of glucose was observed ($p > 0.0125$, Fig. 6b). A secondary direct comparison to test the conditional main effect revealed that Sdha transcript counts were significantly reduced at HG AGE-200 μg/ml compared to HG AGE-0 μg/ml ($p < 0.05$, Fig. 6b). Bcs1l mRNA was significantly reduced at AGE-50 μg/ml, AGE-100 μg/ml, and AGE-200 μg/ml compared to AGE-0 μg/ml ($p < 0.0125$, Fig. 6c). Bcs1l mRNA was also significantly reduced in the HG condition ($p < 0.0125$, Fig. 6c). Neither AGE treatment nor glucose condition altered Cox4i1 mRNA transcript counts ($p > 0.0125$, Fig. 6d). MT-ATP6 mRNA transcript counts were significantly reduced at HG AGE-200 μg/ml compared to HG AGE-0 μg/ml ($p < 0.05$, Fig. 6e), but no effect of glucose was observed ($p > 0.0125$, Fig. 6e).

Protein analysis of mitochondrial complexes. Expression of complex III (UQCRC2) was significantly increased at AGE-200 μg/ml compared to AGE-0 μg/ml ($p < 0.017$, Fig. 7c), but no glucose effect was observed

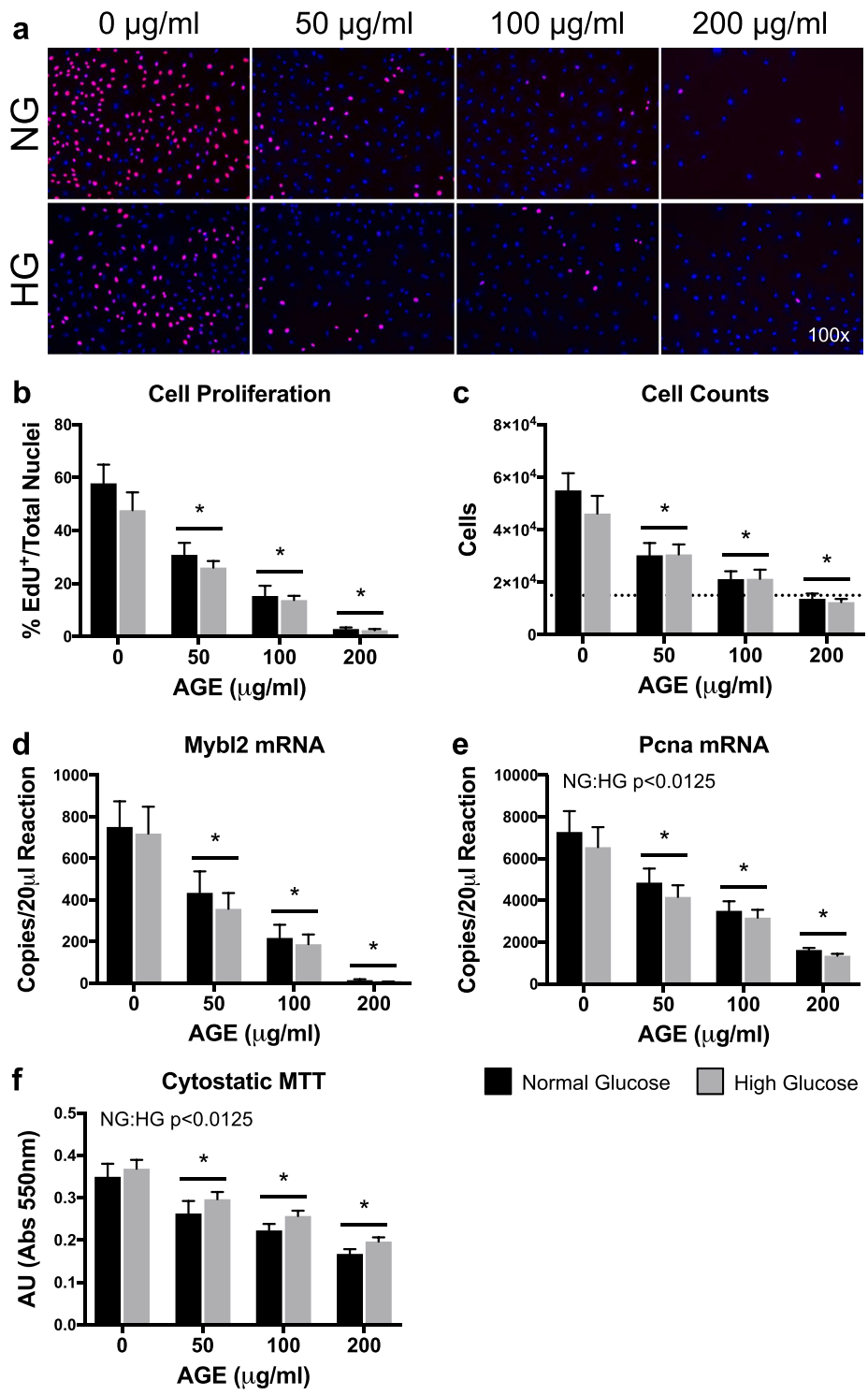

Figure 1. Proliferative Capacity (n = 8). (**a**) Representative images of EdU^+/DAPI overlay after 48 hours of AGE treatment. EdU^+ nuclei are pink and have active DNA synthesis. Blue nuclei (DAPI) do not have active DNA synthesis. (**b**) Graphical representation of EdU images (Panel A). Data represented as ratio of EdU^+ nuclei to total nuclei. (**c**) Cell counts after 48 hours of AGE treatment. Dashed line represents initial seeding density of 15,000 cells. (**d,e**) ddPCR gene transcript counts for Myb-related protein B (Mybl2) and proliferating cell nuclear antigen (Pcna). (**f**) Cytostatic MTT shown as absolute arbitrary absorbance units. *$p < 0.0125$ main effect for AGE vs. AGE-0 µg/ml, mixed effects regression. NG:HG $p < 0.0125$ indicates main effect for glucose condition, mixed effects regression. Data presented as mean ± standard error. ■ Normal Glucose (NG), ■ High Glucose (HG).

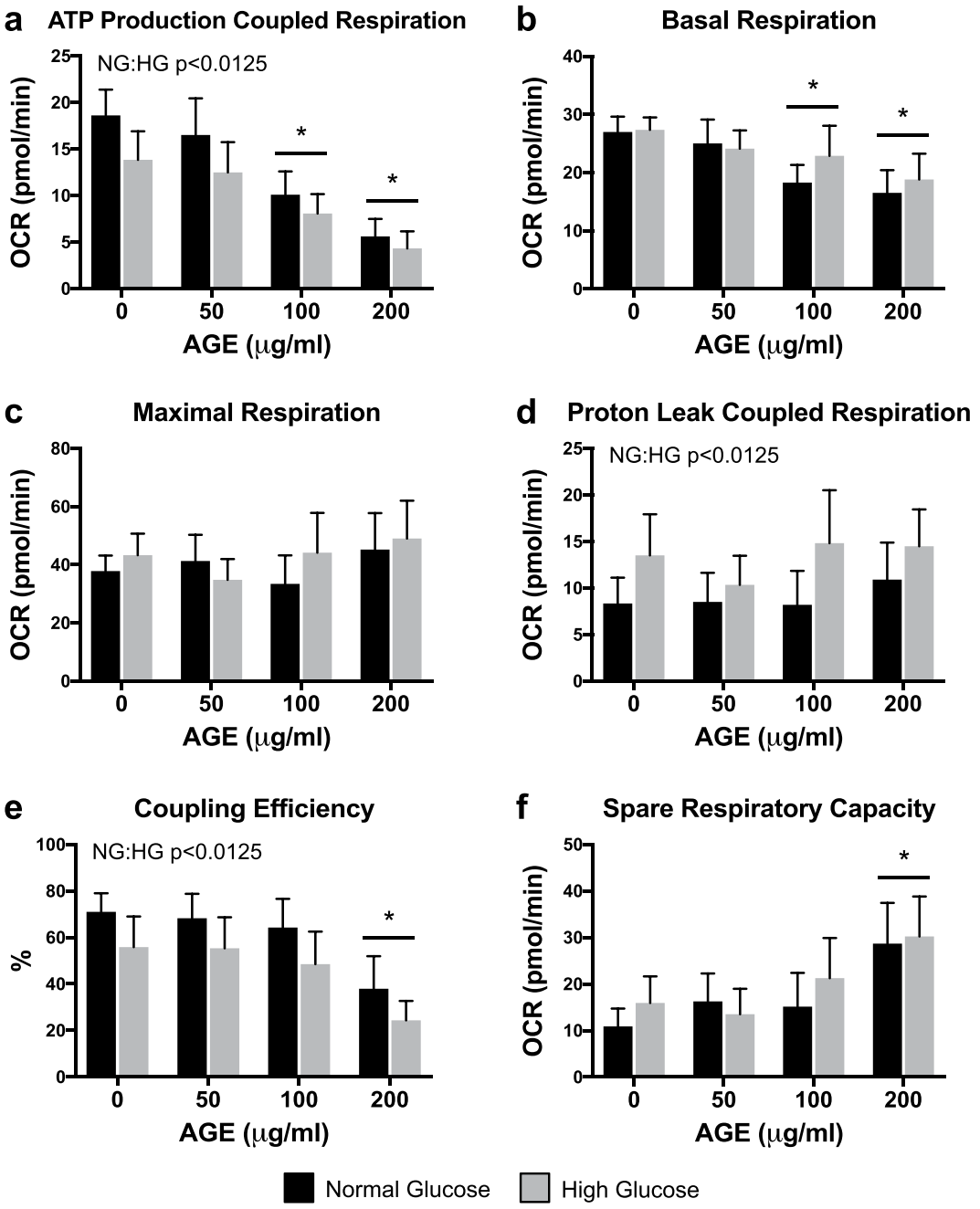

Figure 2. Mitochondrial Stress Tests (n = 8). (**a**–**f**) Mitochondrial parameters as a function of oxygen consumption rate (OCR). *$p < 0.0125$ main effect for AGE vs. AGE-0 μg/ml, mixed effects regression. NG:HG $p < 0.0125$ indicates main effect for glucose condition, mixed effects regression. Data presented as mean ± standard error. ■ Normal Glucose (NG), ■ High Glucose (HG).

($p > 0.017$, Fig. 7c). Expression of complex I (NDUFB8), II (SDHB), IV (MTCO1), or V (ATP5A) were not altered by either AGE treatment or glucose condition ($p > 0.017$, Fig. 7a,b,d,e, respectively). However, a significant interaction between AGE treatment and glucose condition was observed for complex I (NDUFB8) and complex IV (MTCO1) ($p < 0.017$, Fig. 7a,d).

Transcriptional analysis of mitochondrial apoptosis. Bak1 mRNA transcript counts were significantly reduced at AGE-100 μg/ml and AGE-200 μg/ml compared to AGE-0 μg/ml ($p < 0.0125$, Fig. 8a), but no effect of glucose condition was observed ($p > 0.0125$, Fig. 8a). Bax and Casp8 mRNA transcript counts were significantly reduced at HG AGE-200 μg/ml compared to HG AGE-0 μg/ml ($p < 0.05$, Fig. 8b,e, respectively), but no effect of glucose was observed ($p > 0.0125$, Fig. 8b,e, respectively). Bcl2 and Tgfbr3 mRNA transcript counts were significantly reduced at AGE-200 μg/ml compared to AGE-0 μg/ml ($p < 0.0125$, Fig. 8c,f, respectively), but no effect

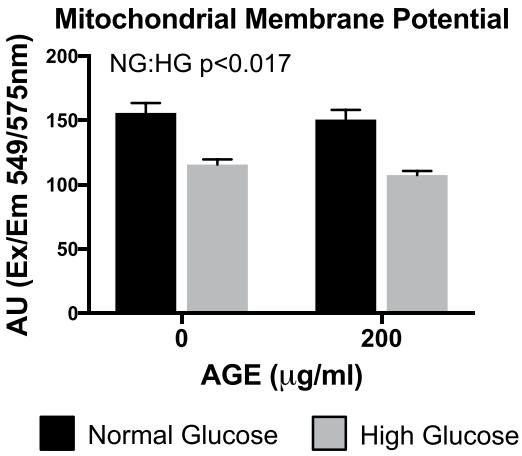

Figure 3. Mitochondrial Membrane Potential (n = 4). NG:HG $p < 0.025$ indicates main effect for glucose condition, mixed effects regression. Data presented as mean ± standard error. ■ Normal Glucose (NG), ■ High Glucose (HG).

of glucose condition was observed ($p > 0.0125$, Fig. 8c,f, respectively). AGE treatment had no effect on Casp3 mRNA ($p > 0.0125$, Fig. 8d), but the HG condition reduced Casp3 mRNA transcript counts ($p < 0.0125$, Fig. 8d).

Superoxide production. Mitochondrial and total ROS/superoxide production were significantly increased at AGE-200 μg/ml compared to AGE-0 μg/ml ($p < 0.025$, Fig. 9a,b, respectively), but no glucose effect was observed in either ($p > 0.025$, Fig. 9).

Discussion

AGE-induced non-enzymatic collagen cross-link formation in the ECM has been proposed to increase tendon stiffness in diabetic individuals[6,7,10]. However, factors contributing to tendon degeneration and collagen fibril disorganization in diabetic tendon have not been extensively characterized. The detrimental effects of AGE associated pathology are well described in non-tendon tissues and have been linked to several diabetic complications such as cardiomyopathy, retinopathy, nephropathy, and endothelial dysfunction[10,20]. In this study, we sought to address the effect of AGEs at the cellular level to better understand factors that may contribute to the disorganization and degeneration of tendon ECM noted in diabetic individuals. Using an *in-vitro* primary cell culture system, we demonstrate dose-dependent AGE-induced reductions in proliferative capacity and mitochondrial ATP production of tendon-derived fibroblasts. Additionally, we demonstrate increased mtDNA content and modifications to mitochondrial complexes and markers of apoptosis after AGE treatment. While previous research has established AGE dependent mitochondrial and proliferative limitations[17,18,21], these data, to the best of our knowledge, are the first to show these impairments in tendon-derived fibroblasts.

Tendon injuries and degenerative pathology are a common and debilitating clinical problem in diabetic individuals[2,3,22–26]. Diabetic tendons are thicker[24,27], and more commonly present with fibril disorganization[2]. Despite convincing epidemiological data, the molecular factors contributing to the development and degenerative process of tendinopathy in diabetic individuals are not well characterized. Much focus has been directed to the influence of elevated glucose on cellular and structural tendon parameters. *In-vitro* and *in-vivo* data have indicated that elevated glucose availability can alter cell signaling dynamics and structural properties in tendon[28–30]. These data suggest that glucose may contribute to tendon pathology, however conflicting reports exist and more conclusive human data is needed to confirm hyperglycemia-associated tendon degeneration in diabetes.

As evidenced, glucose does seem to be implicated in modulation of some tendon cellular and structural properties[28–30], however, the underlying mechanisms influencing tendon degeneration in diabetic patients remain inconclusive. Couppé *et al.*[4] have demonstrated that Achilles tendon Young's modulus (stiffness) is greater in diabetic subjects compared to control subjects, but no difference exists between subjects with well-controlled and poorly controlled diabetes. These data highlight that hyperglycemia is unlikely to be the sole contributor of diabetic tendon pathology. In support of this notion, we explored the role of AGEs on modulation of tendon cellular properties that may consequently interfere with regulation and maintenance of the ECM.

Tendon fibroblast proliferation is a vital component to tendon development, adaptation, and healing[31,32]. An inability of tenocytes to proliferate in the presence of AGEs would significantly precipitate the development of tendinopathy[33]. Tendinopathy is thought to develop, in part, from a failed healing response to minor tendon damage during loading. Specifically, delayed and abnormal healing is a common complication of both type I and type II diabetes[34,35]. As evidence, tendinopathies in diabetic patients are generally more pervasive and can present with more severe degeneration, which may, in part, be driven by prolonged injury status[2,36,37]. We note dramatic impairments to tendon fibroblast proliferative capacity in the presence of AGEs. Our *in-vitro* data demonstrate, in a dose dependent fashion, reduced cell proliferation (EdU) and cell counts after 48 hours of AGE treatment (Fig. 1b,c, respectively). In concert, we demonstrate a reduction in proliferative gene markers, Mybl2 and Pcna, and reduced absorbance values of cytostatic MTT with AGE treatment (Fig. 1d–f, respectively). These data are

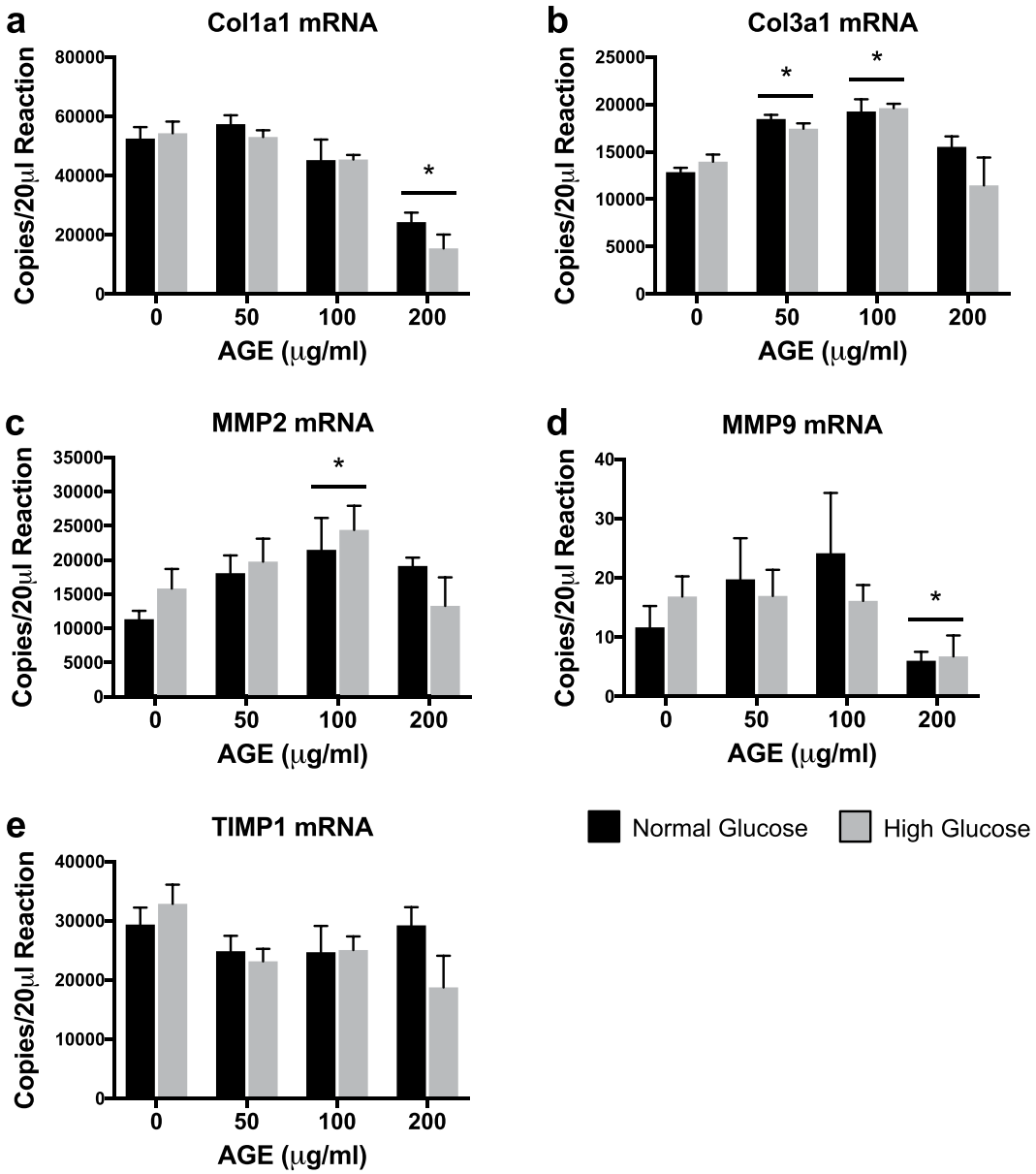

Figure 4. Transcriptional Analysis of Extracellular Matrix Remodeling (n = 4). (**a**–**e**) ddPCR gene transcript counts for Collagen alpha-1(I) chain (Col1a1), Collagen alpha-1(III) chain (Col3a1), Matrix metallopeptidase 2 (MMP2), Matrix metalloproteinase 9 (Col3a1), and Tissue inhibitor of matrix metalloproteinase 1 (TIMP1). *$p < 0.0125$ main effect for AGE vs. AGE-0 μg/ml, mixed effects regression. Data presented as mean ± standard error. ■ Normal Glucose (NG), ■ High Glucose (HG).

in agreement with data from Hu *et al.*[21], which also demonstrates a lack of proliferative capacity in the presence of AGEs. While the HG condition did impact Pcna mRNA and cytostatic MTT (Fig. 1e,f), the primary insult to proliferative capacity appears to be driven by AGE treatment. Impaired proliferation is likely mediated by RAGE signaling[38], but further work is needed to confirm AGE-mediated impairments to tendon fibroblast proliferation and tendon healing.

AGEs have been linked to numerous diabetes related complications and their detrimental effects are well documented in several tissues[10,20]. The primary consequences of AGE-mediated RAGE activation are chronic inflammation, as result of the NF-κB mediated cascade, and oxidative stress, due to NADPH oxidase stimulation. Among resulting complications, reports in other cell types have identified AGE-mediated impairments to mitochondrial function and dynamics[15–18]. Similarly, we report impaired mitochondrial parameters and reduced ATP production-coupled respiration in tendon fibroblasts treated with AGEs (Fig. 2a). The role of ATP is diverse and essential for a multitude of cellular processes including cell proliferation, contraction, and wound healing. Specifically, ATP has been shown to promote biosynthesis of the ECM in intervertebral disk cells[19]. In tendon, the resident fibroblast population maintains the ECM, which is primarily composed of collagen. Due to the energy demanding nature of ECM maintenance, it is possible, that in the presence of AGEs, limited ATP production

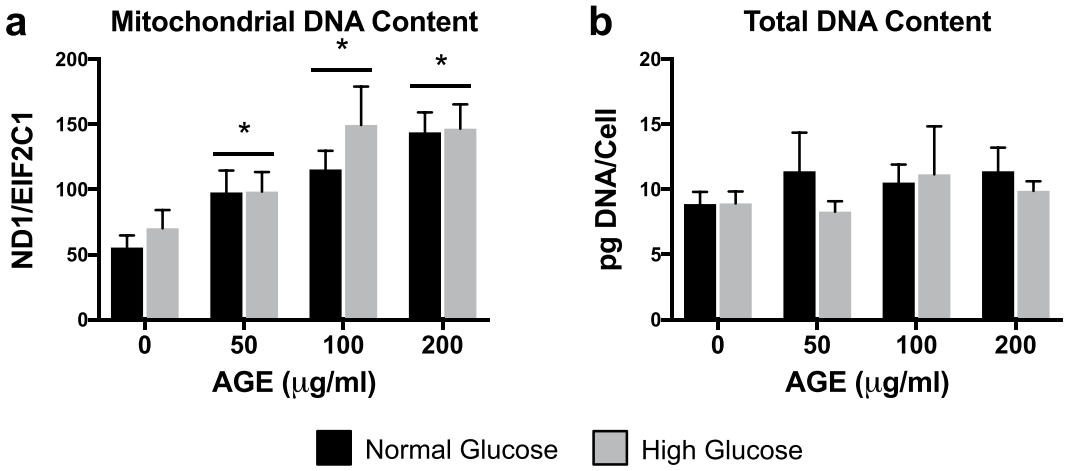

Figure 5. Mitochondrial DNA Content (n = 8). (**a**) mtDNA content quantified by ratio of mitochondrial gene, NADH dehydrogenase subunit 1 (ND1), to nuclear reference gene, protein argonaute-1 (EIF2C1). (**b**) Total DNA content normalized to cell counts. *$p < 0.0125$ main effect for AGE vs. AGE-0 μg/ml, mixed effects regression. Data presented as mean ± standard error. ■ Normal Glucose (NG), ■ High Glucose (HG).

contributes to loss of organization in the ECM, which is commonly noted in diabetic tendon[1–3]. While maximal respiration of tendon fibroblasts was unchanged due to identical XFp seeding density, basal respiration was reduced after AGE treatment (Fig. 2b,c, respectively). In addition to loss of ATP production and reduced basal respiration, we demonstrate that AGEs also impair electron transport coupling efficiency; thereby increasing spare respiratory capacity of AGE treated tendon fibroblasts and indicating overall reduction to electron transport efficiency (Fig. 2e,f, respectively). Interestingly, the HG condition reduced ATP production and coupling efficiency (Fig. 2a,e) and increased proton leak across the inner mitochondrial membrane (Fig. 2d), suggesting that glucose alone can also impact electron transport efficiency. Proton leak across the inner membrane is known to influence mitochondrial membrane potential[39,40]. In agreement with our proton leak data, our analysis revealed that the HG condition reduces mitochondrial membrane potential, however, no effect of AGE is observed (Fig. 3). It is important to note that AGE and/or glucose-mediated mitochondrial impairments are likely not the sole contributor of tendon ECM disorganization. For example, AGEs increase matrix metalloproteinases (MMP) expression and activity, which may contribute in an additive manner to enhanced degeneration in tendon ECM[41].

To address our hypothesis that the presence of AGEs and resulting limited ATP production contribute to loss of organization in the ECM, we completed gene analysis of targets associated with ECM maintenance and remodeling. We note that AGE treatment reduces Col1a1 mRNA expression (Fig. 4a), consistent with previous work which has demonstrated reduced collagen synthesis during AGE treatment in fibroblasts[42]. Col3a1 mRNA expression was however increased with AGE 50 μg/ml and 100 μg/ml, but not at 200 μg/ml (Fig. 4b). Col3a1 expression is upregulated after injury and during the early stages of wound healing[43,44]. It is possible that in our cell culture model, increased Col3a1 mRNA expression in the AGE 50 μg/ml and 100 μg/ml groups was an attempt to overcome the AGE insult to tendon fibroblast collagen production. However, it appears that the potential compensatory response was unsuccessful in the AGE 200 μg/ml group (Fig. 4b). Further, MMPs and tissue inhibitors of metalloproteinases (TIMPs) work to tightly regulate ECM remodeling. Previous work in chondrocyte cell culture has demonstrated an increase to MMP mRNA expression with AGE treatment[41,45]. While we did observe increased MMP2 mRNA expression in the AGE 100 μg/ml group, MMP9 mRNA expression was reduced in the AGE 200 μg/ml group (Fig. 4c,d). Lastly, we did not observe an AGE or glucose effect of TIMP1 mRNA (Fig. 4e). Reduced collagen expression and altered MMP modulation may favor an environment that promotes loss of ECM organization. Future work evaluating post-translational MMP activation and collagen fibril organization is needed to determine the role of AGEs in modulation of tendon ECM.

We also noted increased content of mtDNA after 48 hours of AGE treatment, despite striking reductions to ATP production. mtDNA content can be used as an estimate of mitochondrial volume[46], however, contrary to our hypothesis, 48 hours of AGE treatment resulted in increased mtDNA content in a dose dependent manner independent of glucose condition (Fig. 5a). Based on our findings, it is plausible that the increase in mtDNA in AGE-treated tendon fibroblasts was indicative of a compensatory response to overcome the AGE insult and meet energy demands[47,48]. In support of this theory, cells under oxidative stress have been shown to increase mitochondria and mtDNA[49]. Additionally, Kim *et al.*[48] have demonstrated a relationship between mtDNA content and severity of histopathology in cancerous lesions, suggesting that increased mtDNA content may be used as a measure of DNA injury and pathology. Despite this compensatory response, functional mitochondrial limitations were still evident after 48 hours of AGE treatment. Alternatively, it is possible that AGE-induced limitations to mitochondrial biogenesis may result in failure of tendon fibroblasts to meet energy demands. For example, mtDNA is more susceptible to mutation than nuclear DNA and AGEs have been shown to induce damage to mtDNA, which could ultimately impact mitochondrial biogenesis[50,51]. However, further molecular work is needed to conclusively define the pathway of AGE-mediated mitochondrial damage. To confirm that mtDNA content measurements were not falsely elevated by an increase in total DNA, despite equal DNA loading per PCR reaction, we

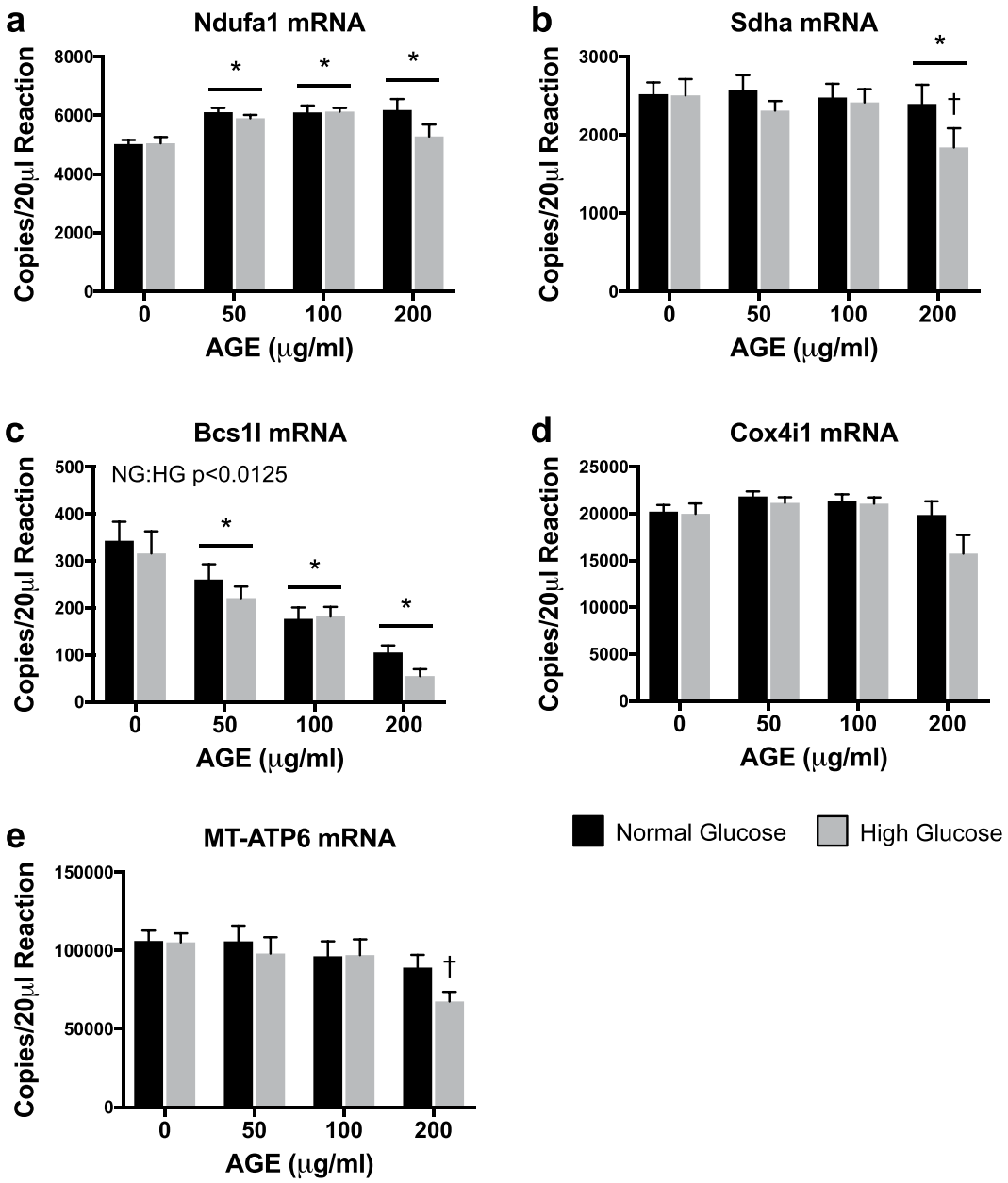

Figure 6. Transcriptional Analysis of Mitochondrial Complexes (n = 8). (**a–e**) ddPCR gene transcript counts for NADH:ubiquinone oxidoreductase subunit A1 (Ndufa1), Succinate dehydrogenase complex flavoprotein subunit A (Sdha), BCS1 homolog, ubiquinol-cytochrome c reductase complex chaperone (Bcs1l), Cytochrome c oxidase subunit 4i1 (Cox4i1), and ATP synthase 6, mitochondrial (MT-ATP6). *$p < 0.0125$ main effect for AGE vs. AGE-0 μg/ml, mixed effects regression. $^{\dagger}p < 0.05$ vs. HG AGE-0 μg/ml, paired t-test. NG:HG $p < 0.0125$ indicates main effect for glucose condition, mixed effects regression. Data presented as mean ± standard error. ■ Normal Glucose (NG), ■ High Glucose (HG).

normalized total DNA yield to cell counts and noted no difference in DNA content with either glucose condition or AGE treatment (Fig. 5b).

Reactive oxygen species (ROS), produced primarily by mitochondria, have been implicated in AGE-mediated cell apoptosis and mitochondrial damage[18,52,53]. To further explore and identify specific targets of the AGE insult, we assessed regulation of electron transport complexes and apoptosis. Analysis of gene transcripts associated with complex I-V (Fig. 6a–e, respectively) of the electron transport chain revealed increased expression of Ndufa1 mRNA (Fig. 6a) and marked reduction of Bcs1l mRNA (Fig. 6c) with AGE treatment. Additionally, the HG condition further reduced Bcs1l mRNA expression (Fig. 6c). Increased Ndufa1 mRNA after AGE treatment may be interpreted as a compensatory response to increase mitochondrial complex I in effort to meet energy demands after the AGE insult. However, Bcs1l mRNA, which encodes mitochondrial complex III, is dramatically reduced in a dose dependent manner after AGE treatment, suggesting that the AGE insult may be targeted to complex

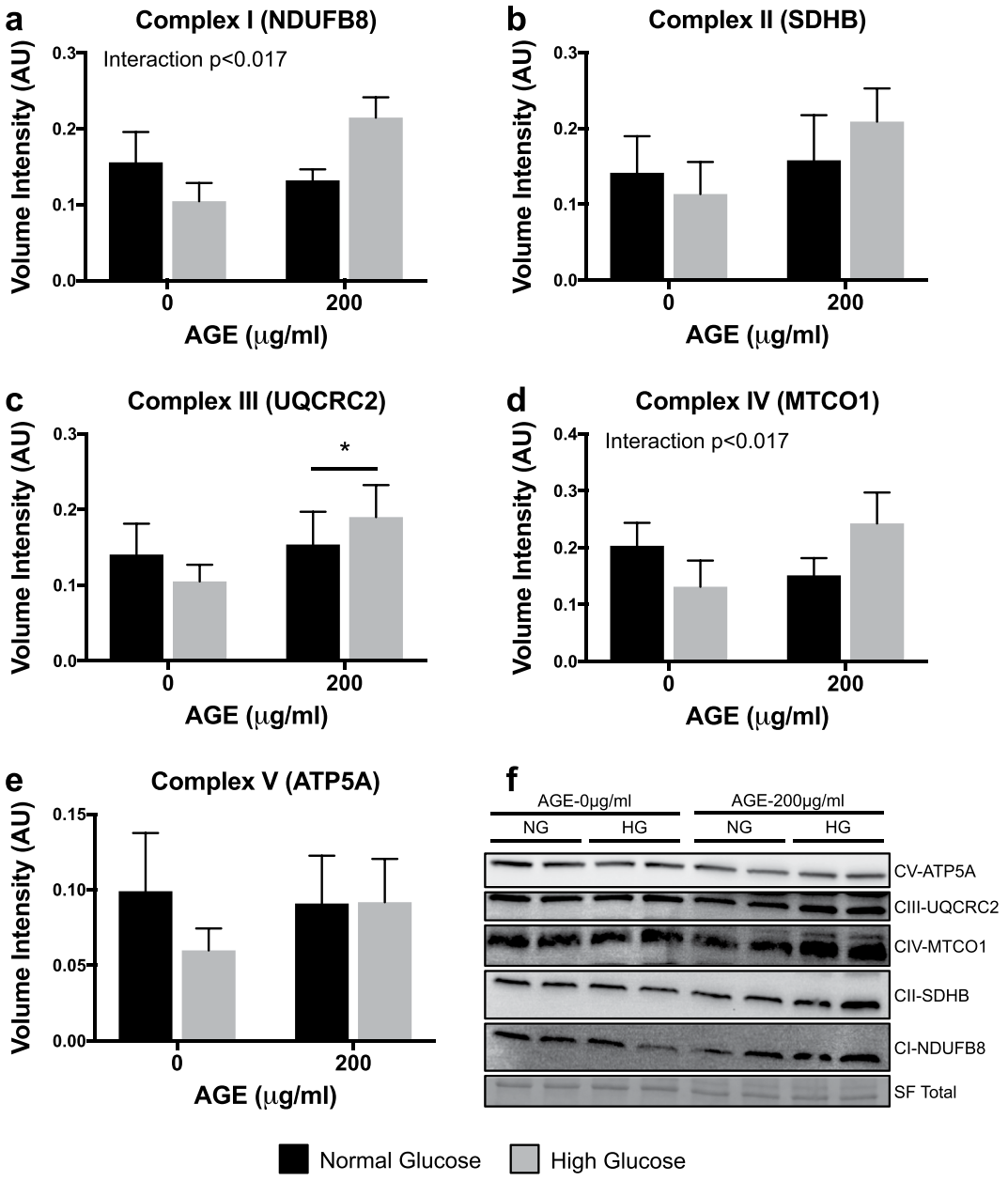

Figure 7. Protein Analysis of Mitochondrial Complexes (n = 4). (**a**–**e**) OXPHOS protein expression for mitochondrial complex I (NDUFB8), complex II (SDHB), complex III (UQCRC2), complex IV (MTCO1), and complex V (ATP5A). F. Representative cropped blot images (displayed in order of molecular weight) including Stain Free (SF) UV visualized total protein. For each sample, all five targets were probed on the same blot. Individual representative images of targets from different parts of the same blot are cropped due to different exposure times required for each target (Signal Accumulation Mode). Representative images were chosen from two of the four blots and both full-length blots with the multiple exposures are presented in Supplementary Fig. 1. *$p < 0.017$ main effect for AGE vs. AGE-0 μg/ml, mixed effects regression. Interaction $p < 0.017$, significant interaction between AGE treatment and glucose condition. Data presented as mean ± standard error. ■ Normal Glucose (NG), ■ High Glucose (HG).

III. Lastly, Sdha and MT-ATP6 mRNA, coding for mitochondrial complex II and complex V (ATP synthase), respectively, were reduced in the HG AGE-200 μg/ml group compared to HG AGE-0 μg/ml (Fig. 6b,c, respectively). A direct comparison was made between HG AGE-0 μg/ml and HG AGE-200 μg/ml to test the conditional main effect and reveal a significant reduction to Sdha and MT-ATP6 mRNA, suggesting that both AGE treatment and HG condition were contributing to this reduction. Cox4i1 (complex IV, Fig. 6d) was not impacted by either AGE treatment or HG condition. While these gene data provide indication that AGEs may indeed have targeted effects to the electron transport chain, protein analysis revealed a significant AGE main effect for only complex III (UQCRC2) (Fig. 7c). Additionally, complex III protein expression was increased with AGE exposure, while

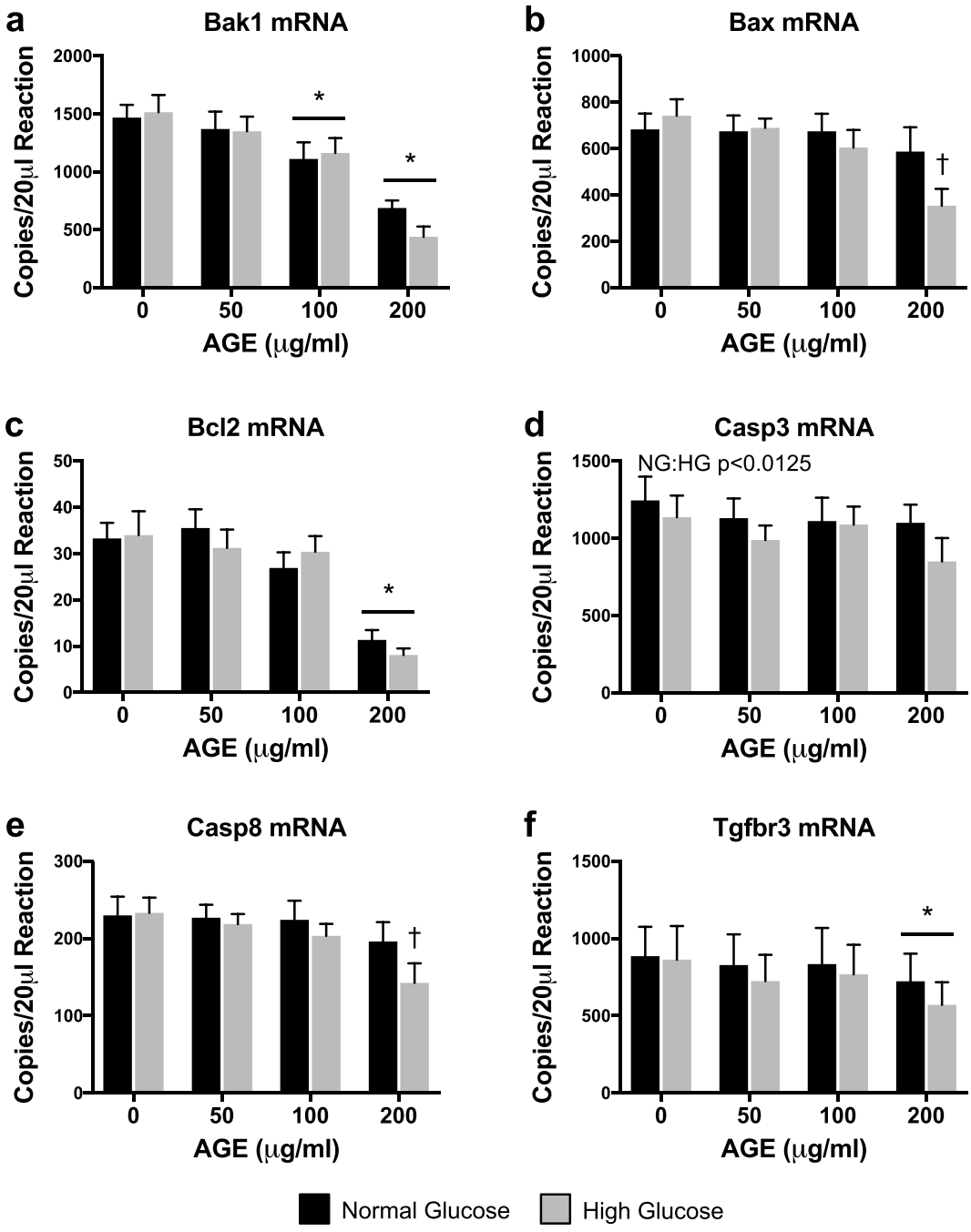

Figure 8. Transcriptional Analysis of Mitochondrial Apoptosis (n = 8). (**a**–**f**) ddPCR gene transcript counts for BCL2-antagonist/killer 1 (Bak1), BCL2 associated X, apoptosis regulator (Bax), B-cell lymphoma 2, apoptosis regulator (Bcl2), Caspase 3 (Casp3), Caspase 8 (Casp8), and Transforming growth factor beta receptor 3 (Tgfbr3). *$p < 0.0125$ main effect for AGE vs. AGE-0 μg/ml, mixed effects regression. †$p < 0.05$ vs. HG AGE-0 μg/ml, paired t-test. NG:HG $p < 0.0125$ indicates main effect for glucose condition, mixed effects regression. Data presented as mean ± standard error. ■ Normal Glucose (NG), ■ High Glucose (HG).

complex III mRNA expression was reduced. Lack of response to remaining complexes and discrepancies between gene and protein analysis may be attributed to the acute duration of AGE exposure. Further, an interaction between AGEs and glucose condition was observed in complex I (NDUFB8, Fig. 7a) and complex IV (MTCO1, Fig. 7d). These results merit further work to discover mechanistic pathways by which AGEs limit mitochondrial function during long-term AGE exposure.

To assess the impact of AGEs on mitochondrial-related tendon fibroblast apoptosis, we completed analysis of associated gene transcripts and measurement of superoxide production. Transcript counts of pro-apoptotic gene Bak1 were reduced with AGE treatment (Fig. 8a). Additionally, pro-apoptotic Bax mRNA expression was reduced

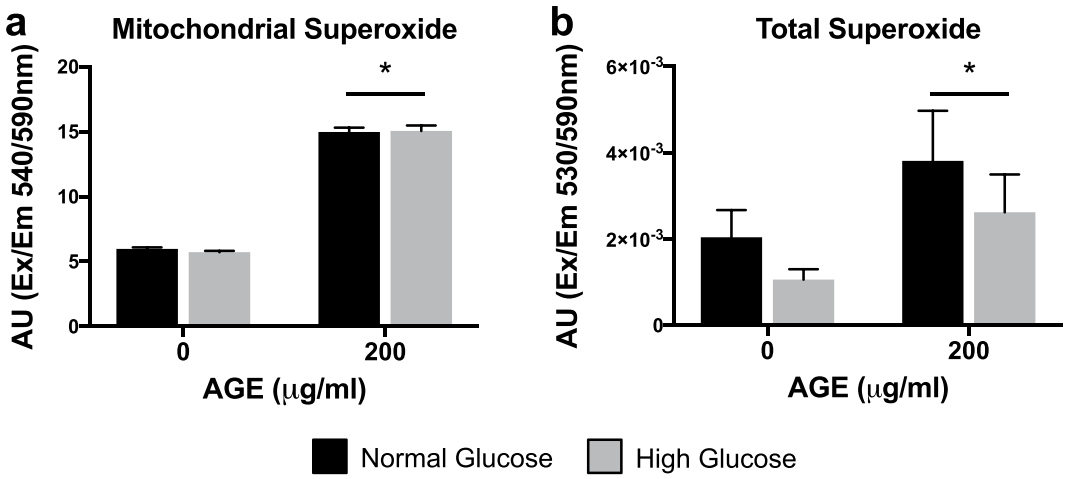

Figure 9. ROS/Superoxide Production (n = 4). (**a**) Mitochondrial Superoxide. (**b**) Total Superoxide. *$p < 0.025$ main effect for AGE vs. AGE-0 μg/ml, mixed effects regression. Data presented as mean of arbitrary fluorescence units ± standard error. ■ Normal Glucose (NG), ■ High Glucose (HG).

only in the HG AGE-200 μg/ml group compared to HG AGE-0 μg/ml (Fig. 8b). Although these findings are contrary to previous work[21], it is possible that these may be compensatory responses to AGE-mediated apoptotic signals. In agreement with previous work by Hu *et al.*[21], expression of Bcl2 mRNA, an anti-apoptotic mediator, was reduced with AGE treatment (Fig. 8c). Previous reports have indicated an inverse relationship between Bcl2 and ROS, where ROS may act to reduce expression of Bcl2 and sensitize cells to apoptosis[54]. In agreement, our analysis of superoxide, the primary mitochondrial- derived reactive oxygen species[55], demonstrates increased production of both mitochondrial derived and total superoxide after AGE treatment (Fig. 9). Further, cytochrome c release is suppressed by Bcl2, but is promoted by Bak1 and Bax. Cytochrome c release will ultimately result in caspase activation[56]. Previous reports indicate AGE treatment induces caspase activation[21,57], however we did not note any AGE-induced changes to Casp3 mRNA (Fig. 8d) but did note reduced Casp8 mRNA in the HG AGE-200 μg/ml group compared to HG AGE-0 μg/ml (Fig. 8e). Finally, transcript counts of Tgfbr3 were reduced with AGE treatment (Fig. 8f). Tgfbr3 overexpression has been shown to increase Bax and Bcl2 expression, as well as promote activation of caspase 3[58]. Casp3 mRNA expression was reduced in the HG condition and was the only target associated with apoptosis to be affected by glucose (Fig. 8d). From these data, it is evident that AGEs alter transcriptional regulation of gene transcripts associated with apoptosis, however, we are limited in our interpretation and further post-translational and activity assays are needed to define the precise mechanisms by which AGEs may induce apoptosis in diabetic tendinopathy.

In summary (Fig. 10), we demonstrate that AGEs, which are elevated in serum of diabetic individuals, impair proliferative capacity, ATP production, and electron transport chain efficiency. Additionally we demonstrate that AGEs alter regulation of mitochondrial complex expression and gene transcripts associated with apoptosis. While the HG condition did impact some mitochondrial parameters, AGEs appear to be the primary insult and may be responsible for the development of the diabetic tendon phenotype. This work provides new insights to the pathophysiology of tendon ECM in diabetic patients. However, future *in-vivo* and mechanistic work is needed to determine whether controlling serum AGEs in diabetic patients can reduce risk of degenerative tendinopathy.

Methods

AGE preparation. Glycolaldehyde-derived AGEs were generated under sterile conditions as described by Valencia *et al.*[59]. Briefly, sterile filtered 30% BSA solution (Sigma, St. Louis, MO) was incubated with 70 mM glycolaldehyde dimer (Sigma) in sterile PBS without calcium chloride and magnesium chloride for three days at 37 °C. After incubation, the AGE product was dialyzed against sterile PBS for 24 hours at 4 °C using gamma-irradiated 10 kDa cut-off cassettes (Thermo Scientific, Waltham, MA) to remove unreacted glycolaldehyde. Unmodified control BSA was prepared similarly, without the addition of glycolaldehyde dimer. Protein concentration was determined by BCA assay (Thermo Scientific) and absence of endotoxin (<0.25Eu/ml) was confirmed via the LAL gel-clot assay (GenScript, Piscataway, NJ).

Extent of AGE modification. Extent of BSA modification was confirmed by fluorescence, absorbance, and loss of primary amines[59–62]. AGE-BSA and Control-BSA were diluted to 1 mg/ml in PBS and fluorescent spectra and absorbance were recorded at 335 nm excitation/420 nm emission and 340 nm, respectively (Molecular Devices, San Jose, CA). For determination of loss of primary amines AGE-BSA and Control-BSA were diluted to 0.2 mg/ml in PBS. An equal volume of ortho-phthalaldehyde solution (Sigma) was added and fluorescent spectrum was recorded at 340 nm excitation/455 nm emission (Molecular Devices). A standard curve of 0 to 0.2 mg/ml of BSA that did not undergo 37 °C incubation was used to generate a standard curve of free amine content and data was normalized to represent percentage of amine terminals remaining with reference to the standard curve[59]. Respective fluorescence or absorbance values of PBS alone were subtracted from all data. AGE-BSA

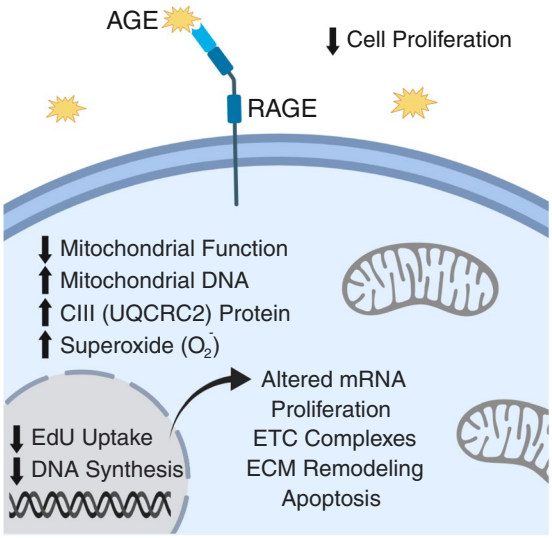

Figure 10. Summary of Major AGE-Mediated Findings. Figure created with BioRender.

fluorescence was increased to 697.78 arbitrary units (AU) compared to −0.72 AU for control BSA. Absorbance readings were completed to determine the extent of glycation. AGE-BSA showed increased glycation with absorbance readings of 0.682 AU compared to 0.01 AU for control BSA. Finally, AGE-BSA primary amine terminals underwent complete modification (−0.03% accessible amine terminals remaining), while control BSA retained 81.48% of accessible amine terminals. Spectra and absorbance values of PBS alone were subtracted from data but resulted in negative values for fluorescent-based detection because the spectra of PBS alone was greater than the obtained sample values. Negative values were interpreted as zero, and extent of modification was similar to previous reports[59].

Animal protocol. This study was approved by the Purdue University Institutional Animal Care and Use Committee and all animals were cared for in accordance with the recommendations in the Guide for the Care and Use of Laboratory Animals[63]. Eight-week-old female Sprague-Dawley rats (n = 8,256.43 ± 5.19 g) were purchased from Charles River Laboratories (Wilmington, MA) and maintained for an additional eight weeks. Rats were housed on a 12-hour light-dark cycle and provided access to standard rat chow and water ad libitum. At sixteen weeks, rats were euthanized by decapitation after CO_2 inhalation.

Tendon fibroblast isolation and cell culture. Tendon-derived fibroblasts were isolated from the Achilles tendons of eight rats. After euthanasia, Achilles tendons were carefully excised and trimmed of remaining muscle and fascia. The tendon was rinsed with sterile PBS, finely minced, placed in DMEM containing 0.2% type I collagenase, and incubated in a 37 °C shaking water bath for four hours. After tissue digestion, the cell suspension was filtered through a 100 μm mesh filter, pelleted by centrifugation, resuspended in 5.5 mM glucose DMEM containing 10% FBS, 1% sodium pyruvate (Sigma), and 1% penicillin/streptomycin (Thermo Scientific) and plated in 100 mm collagen coated dishes. After reaching ~75–80% confluence, tendon fibroblasts were subcultured with either normal glucose (NG, 5.5 mM) DMEM (Sigma) or high glucose (HG, 25 mM) DMEM (Sigma) for a minimum of one passage to allow for glucose condition acclimation. Tendon fibroblasts were then seeded into 6-well, 24-well, or 96-well collagen coated culture plates and treated for 48 hours with 0, 50, 100, and 200 μg/ml of AGEs within both glucose conditions. The 0 μg/ml AGE group was treated with 200 μg/ml of unmodified control BSA. Tendon fibroblasts from passage 2–4 were used for all experiments.

Proliferative capacity. Proliferative capacity was assessed by cell counts, cytostatic MTT, and incorporation of synthetic nucleoside 5-ethynyl-2′-deoxyuridine (EdU). After AGE treatment in 6-well plates, cells were enzymatically released and manually counted with a hemocytometer. Cell counts were completed in duplicate and normalized to total volume in which cells were resuspended. For cytostatic MTT analysis, cells cultured in a 96-well plate were incubated with MTT reagent (5 mg/ml, VWR, Radnor, PA) for the final 90 minutes of AGE treatment. Formazan crystals were solubilized with DMSO and absorbance was read at 550 nm (Multiskan, Thermo Scientific). Each assay was completed in duplicate and data was represented as absolute arbitrary absorbance units. Cells were labeled with 2.5 μM EdU (Carbosynth, Newbury, UK) during the final 12 hours of AGE treatment. EdU is a thymidine analog that incorporates during active DNA synthesis and is used to mark proliferating cells. Fixed cells (4% PFA) were stained with DAPI, and EdU was visualized via the Click-iT method (100 mM Tris-HCl pH 8.5, 1 mM $CuSO_4$, 2.5 μM red-fluorescent tetramethylrhodamine azide, and 100 mM ascorbic acid; Thermo Scientific)[64]. Fluorescent images were captured using a DMI 6000B microscope (Leica, Wetzlar, Germany) with a 10x objective and MetaMorph software (Molecular Devices). EdU data was analyzed using the ImageJ Multi-Point Tool (National Institutes of Health, Bethesda, Maryland) and is reported as a ratio of EdU^+ nuclei to total nuclei from two fields-of-view within each treatment.

Gene Symbol	Description	Gene ID
Bak1	BCL2-antagonist/killer 1	116502
Bax	BCL2 associated X, apoptosis regulator	24887
Bcl2	B-cell lymphoma 2, apoptosis regulator	24224
Bcs1l	BCS1 homolog, ubiquinol-cytochrome c reductase complex chaperone	301514
Casp3	Caspase 3	25402
Casp8	Caspase 8	64044
Col1a1	Collagen alpha-1(I) chain	29393
Col3a1	Collagen alpha-1(III) chain	84032
Cox4i1	Cytochrome c oxidase subunit 4i1	29445
MMP2	Matrix metallopeptidase 2	81686
MMP9	Matrix metalloproteinase 9	84687
MT-ATP6	ATP synthase 6, mitochondrial	26197
Mybl2	MYB proto-oncogene like 2	296344
Ndufa1	NADH:ubiquinone oxidoreductase subunit A1	363441
Pcna	Proliferating cell nuclear antigen	25737
Sdha	Succinate dehydrogenase complex flavoprotein subunit A	157074
Tfgbr3	Transforming growth factor beta receptor 3	29610
TIMP1	Tissue inhibitor of matrix metalloproteinase 1	116510

Table 1. ddPCR Gene Targets.

Mitochondrial stress tests. Tendon fibroblasts were treated for 48 hours prior to being plated (8,000 cells) into collagen coated XFp cell culture miniplates (Seahorse Bioscience, Agilent, Santa Clara, CA). Cultured cells from each treatment condition were reseeded in duplicate, allowed to attach to the miniplates, and washed twice in pre-warmed XF base medium (Agilent). Miniplates were then incubated in XF base medium (1 mM sodium pyruvate, 2 mM glutamine, and either 5.5 mM or 25 mM glucose) for one hour in a 37 °C incubator without CO_2 to allow plate outgassing. Mitochondrial stress experiments were completed on an XFp extracellular flux analyzer (Agilent) with the Mito Stress Test Kit (Agilent). Chemicals (1 μM oligomycin, 0.5 μM carbonyl cyanide-4-(trifluoromethoxy)phenylhydrazone (FCCP), 0.5 μM rotenone, and 0.5 μM antimycinA) were preloaded into cartridge ports and injected in succession during measurement of oxygen consumption rate (OCR).

Mitochondrial membrane potential. Mitochondrial membrane potential ($\Delta\psi m$) was determined using a commercially available tetramethylrhodamine (TMRE) assay (113852, Abcam, Cambridge, MA). Briefly, after 48 hours of AGE treatment, cultured cells were seeded in duplicate (8,000 cells) into collagen coated black 96-well microplates with clear bottoms, allowed to attach, and treated with 1 μM of TMRE for 30 minutes at 37 °C. After incubation, wells were washed with 0.2% BSA in PBS and fluorescence was recorded at 549 nm excitation/575 nm emission (Molecular Devices). Depolarization controls were treated with 20 μM FCCP for 15 minutes prior to addition of TMRE.

Gene expression analysis. Total RNA for gene expression analysis was isolated after AGE treatment using the Direct-zol RNA Miniprep kit (Zymo Research). On-column DNase digestion was completed on all samples prior to elution of RNA. RNA concentration was determined using a NanoDrop 2000 (Thermo Scientific). Quality of RNA was assessed using the 260/280 and 260/230 ratios. Reverse transcription (iScript, BioRad) was completed to produce complementary DNA from 100 ng of RNA. Absolute quantification of mRNA target transcripts was completed using the ddPCR platform (BioRad) with validated probe-based assays (BioRad) as previously described[30]. For optimal detection, Col1a1 and Col3a1 reactions contained 0.55 ng of cDNA, while MMP2, MMP9, and TIMP1 contained 4.4 ng of cDNA[30]. All other target PCR reactions contained 2.2 ng of cDNA. A list of measured gene targets is provided in Table 1.

Mitochondrial DNA content. mtDNA content was quantified by ratio of a target mitochondrial gene, NADH dehydrogenase subunit 1 (ND1), to nuclear reference gene, protein argonaute-1 (EIF2C1)[65,66]. Total DNA was isolated using the Quick-DNA Microprep kit (Zymo Research, Irvine, CA). DNA concentration was determined using a NanoDrop 2000 (Thermo Scientific) and serial diluted to 1 ng/μl. A droplet digital PCR (ddPCR) method was used to complete quantification of absolute copy number of both ND1 and EIF2C1. Reactions were prepared in duplex format, in a final volume of 20 μl with 2x ddPCR Supermix for Probes (No dUTP) (BioRad, Hercules, CA), 20x reference probe ND1 labeled with FAM (BioRad), 20x reference probe EIF2C1 labeled with HEX (BioRad), 5 ng of DNA, 1 μl of HindIII enzyme (FastDigest, Thermo Scientific), and nuclease-free water. The assembled reaction was incubated at room temperature for 20 minutes to permit digestion with the HindIII restriction enzyme. After digestion, droplets were generated from prepared PCR reactions using Droplet

Figure	AGE-0 μg/ml vs. AGE-50 μg/ml	AGE-0 μg/ml vs. AGE-100 μg/ml	AGE-0 μg/ml vs. AGE-200 μg/ml	Normal vs. High Glucose	Interaction
1B	4×10^{-5}	3×10^{-14}	$<2 \times 10^{-16}$	NS	N/A
1C	1×10^{-8}	5×10^{-15}	$<2 \times 10^{-16}$	NS	N/A
1D	1.5×10^{-10}	$<2 \times 10^{-16}$	$<2 \times 10^{-16}$	NS	N/A
1E	4×10^{-9}	2×10^{-15}	$<2 \times 10^{-16}$	7×10^{-3}	N/A
1F	5×10^{-9}	1.5×10^{-14}	$<2 \times 10^{-16}$	8×10^{-4}	N/A
2A	NS	3×10^{-7}	2×10^{-14}	1×10^{-3}	N/A
2B	NS	9×10^{-6}	5×10^{-10}	NS	N/A
2C	NS	NS	NS	NS	N/A
2D	NS	NS	NS	2×10^{-3}	N/A
2E	NS	NS	1×10^{-14}	1×10^{-7}	N/A
2F	NS	NS	3×10^{-4}	NS	N/A
3	N/A	N/A	NS	2.8×10^{-7}	N/A
4A	NS	NS	5×10^{-11}	NS	N/A
4B	5×10^{-4}	1.4×10^{-5}	NS	NS	N/A
4C	NS	3×10^{-4}	NS	NS	N/A
4D	NS	NS	7×10^{-3}	NS	N/A
4E	NS	NS	NS	NS	N/A
5A	6×10^{-7}	1×10^{-12}	2×10^{-15}	NS	N/A
5B	NS	NS	NS	NS	N/A
6A	6×10^{-6}	8×10^{-7}	7×10^{-5}	NS	N/A
6B	NS	NS	5×10^{-3}	NS	N/A
6C	2×10^{-5}	1×10^{-11}	$<2 \times 10^{-16}$	1×10^{-2}	N/A
6D	NS	NS	NS	NS	N/A
6E	NS	NS	NS	NS	N/A
7A	N/A	N/A	NS	NS	1.2×10^{-2}
7B	N/A	N/A	NS	NS	NS
7C	N/A	N/A	1.3×10^{-2}	NS	NS
7D	N/A	N/A	NS	NS	2.8×10^{-3}
7E	N/A	N/A	NS	NS	NS
8A	NS	9×10^{-7}	$<2 \times 10^{-16}$	NS	N/A
8B	NS	NS	NS	NS	N/A
8C	NS	NS	7×10^{-10}	NS	N/A
8D	NS	NS	NS	1.1×10^{-2}	N/A
8E	NS	NS	NS	NS	N/A
8F	NS	NS	1×10^{-4}	NS	N/A
9A	N/A	N/A	5.26×10^{-16}	NS	N/A
9B	N/A	N/A	8.6×10^{-3}	NS	N/A

Table 2. Summary of p-values for Statistical Findings. NS = Not Significant. N/A = Not Tested.

Generation Oil for Probes (BioRad) on a QX200 Droplet Generator (BioRad), transferred to a deep-well 96-well plate, and amplified (95 °C-10 minutes, 1 cycle; 94 °C-30 seconds and 60 °C-90 seconds, 40 cycles; 98 °C-10 minutes, 1 cycle) on a C1000 thermal cycler (BioRad). At completion of end-point PCR, absolute quantification of PCR products was completed on a QX200 Droplet Reader (BioRad) with QuantaSoft Software Version 1.7 (BioRad) and reported as a ratio of positive ND1/EIF2C1 counts per 20 μl reaction.

Protein expression. Cultured cells were lysed in RIPA buffer containing 50 mM Tris-HCl, 150 mM NaCl, 2 mM EDTA, 2 mM EGTA, 0.5% sodium deoxycholate, 1% Triton X-100, 0.1% SDS, 50 mM NaF, 0.2 mM Na_3VO_4, and 0.2% protease inhibitor cocktail (Sigma). Samples were prepared as described previously[67]. Equal amounts of protein (15 μg) were separated in duplicate on an Any-kD TGX polyacrylamide gel (BioRad). Protein was transferred to a PVDF membrane (TransBlot Turbo, BioRad) and blocked for 24 hours at 4 °C in 5% blotting-grade blocker (BioRad). Blots were incubated in primary OXPHOS antibody (1:1000, 110413, Abcam) and then HRP-conjugated goat anti-mouse antibody (1:5000, 31430, Invitrogen), each for 2 hours at room temperature. Bands of interest were compared against positive control (Rat Heart Mitochondria, Abcam) and all targets were probed on the same membrane, but required different exposure times using signal accumulation mode (ChemiDoc, BioRad). Volume intensity analysis of matched exposure duration for each target was completed using Image Lab Version 6.0.1 (BioRad). Total protein volume intensity obtained by UV activated Stain-Free imaging was used for data normalization.

Superoxide production. Mitochondrial ROS/superoxide production was determined using a commercially available fluorometric assay (219943, Abcam). Briefly, after 48 hours of AGE treatment, cultured cells were seeded in duplicate (8,000 cells) into collagen coated black 96-well microplates with clear bottoms, allowed to attach, and treated with MitoROS 580 stain for 30 minutes at 37 °C. Fluorescence was recorded at 540 nm excitation/590 nm emission (Molecular Devices). Total ROS/superoxide production was determined by dihydroethidium (DHE) derived fluorescence. Cultured cells were detached, pelleted, and resuspended in Hank's Balanced Salt Solution. An aliquot was saved for determination of cell concentration. DHE (Thermo Scientific) was added at final concentration of 10 μM and samples were incubated with shaking at 37 °C for 30 minutes[68–70]. Fluorescent spectrum was recorded at 530 nm excitation/590 nm emission (Molecular Devices) and fluorescence units were normalized to cell concentration.

Statistical analysis. Statistical analyses on the four main effect contrasts of interest (50 μg/ml AGE vs. 0 μg/ml AGE, 100 μg/ml AGE vs. 0 μg/ml AGE, 200 μg/ml AGE vs. 0 μg/ml AGE, and HG vs. NG) for each outcome variable proceeded via a mixed effects regression model with consideration of technical data replicates and random effects to account for the tendon fibroblast donor rats. Regression models were fit to the data using the lmer function in R. The Kenward-Roger F-test was performed to determine whether the main effects regression model or the "full" model containing both main effects and two-factor interactions between the AGE and glucose contrasts should be fitted. Validity of the assumptions for the models were assessed via standard regression diagnostics. Specifically, the standardized residuals were examined to assess whether they were approximately Normally distributed, centered at zero, and did not exhibit any patterns with respect to the predictor variables. If assumptions appeared invalid for the original scale, the logarithmic and square root transformations were considered. After identifying a model that provided a good fit to the outcome data, hypothesis tests were performed for the contrasts using Satterthwaite's method, and confidence intervals were created using the bootstrap. Hypothesis tests for the contrasts use a Bonferroni-adjusted significance level of $\alpha = 0.05/4 = 0.0125$ (Figs 1, 2, 4–6 and 8) or $\alpha = 0.05/2 = 0.025$ (Figs 3, 9) or $\alpha = 0.05/3 = 0.017$ (Fig. 7) separately across the different outcome variables to account for the multiple comparisons of the specified final models. Certain specified, direct comparisons between two specific groups were performed via the paired t-test in R with $\alpha = 0.05$ to test conditional main effects, where HG was conditioned for testing the AGE contrast of interest. Summary of applied contrasts and exact p-values for significant findings are provided in Table 2. Figures were generated in Prism 7.0 (GraphPad, La Jolla, CA) and are represented as mean ± standard error.

Data Availability

C.C.C has access to all data and data is available upon request.

References

1. Abate, M., Salini, V. & Schiavone, C. Achilles tendinopathy in elderly subjects with type II diabetes: the role of sport activities. *Aging clinical and experimental research* **28**, 355–358, https://doi.org/10.1007/s40520-015-0391-7 (2016).
2. Batista, F. *et al.* Achilles tendinopathy in diabetes mellitus. *Foot Ankle Int* **29**, 498–501, https://doi.org/10.3113/fai.2008.049810.3113/fai-2008-0498 (2008).
3. Grant, W. P. *et al.* Electron microscopic investigation of the effects of diabetes mellitus on the Achilles tendon. *J Foot Ankle Surg* **36**, 272–278, discussion 330 (1997).
4. Couppe, C. *et al.* Human Achilles tendon glycation and function in diabetes. *Journal of applied physiology* **120**, 130–137, https://doi.org/10.1152/japplphysiol.00547.2015 (2016).
5. Lin, T. T. *et al.* The effect of diabetes, hyperlipidemia, and statins on the development of rotator cuff disease: a nationwide, 11-year, longitudinal, population-based follow-up study. *Am J Sports Med* **43**, 2126–2132, https://doi.org/10.1177/0363546515588173 (2015).
6. Eriksen, C. *et al.* Systemic stiffening of mouse tail tendon is related to dietary advanced glycation end products but not high-fat diet or cholesterol. *Journal of applied physiology* **117**, 840–847, https://doi.org/10.1152/japplphysiol.00584.2014 (2014).
7. Monnier, V. M. *et al.* Cross-linking of the extracellular matrix by the maillard reaction in aging and diabetes: an update on "a puzzle nearing resolution". *Annals of the New York Academy of Sciences* **1043**, 533–544, https://doi.org/10.1196/annals.1333.061 (2005).
8. Reddy, G. K., Stehno-Bittel, L. & Enwemeka, C. S. Glycation-induced matrix stability in the rabbit achilles tendon. *Archives of biochemistry and biophysics* **399**, 174–180, https://doi.org/10.1006/abbi.2001.2747 (2002).
9. Reddy, G. K. Cross-linking in collagen by nonenzymatic glycation increases the matrix stiffness in rabbit achilles tendon. *Experimental diabesity research* **5**, 143–153, https://doi.org/10.1080/15438600490277860 (2004).
10. Singh, V. P., Bali, A., Singh, N. & Jaggi, A. S. Advanced glycation end products and diabetic complications. *The Korean journal of physiology & pharmacology: official journal of the Korean Physiological Society and the Korean Society of Pharmacology* **18**, 1–14, https://doi.org/10.4196/kjpp.2014.18.1.1 (2014).
11. Kierdorf, K. & Fritz, G. RAGE regulation and signaling in inflammation and beyond. *Journal of leukocyte biology* **94**, 55–68, https://doi.org/10.1189/jlb.1012519 (2013).
12. Brownlee, M. Biochemistry and molecular cell biology of diabetic complications. *Nature* **414**, 813–820, https://doi.org/10.1038/414813a (2001).
13. Giardino, I., Edelstein, D. & Brownlee, M. Nonenzymatic glycosylation *in vitro* and in bovine endothelial cells alters basic fibroblast growth factor activity. A model for intracellular glycosylation in diabetes. *The Journal of clinical investigation* **94**, 110–117, https://doi.org/10.1172/jci117296 (1994).
14. Skovgaard, D. *et al.* An advanced glycation endproduct (AGE)-rich diet promotes accumulation of AGEs in Achilles tendon. *Physiological reports* **5**, https://doi.org/10.14814/phy2.13215 (2017).
15. Nelson, M. B. *et al.* Cardiomyocyte mitochondrial respiration is reduced by receptor for advanced glycation end-product signaling in a ceramide-dependent manner. *American journal of physiology. Heart and circulatory physiology* **309**, H63–69, https://doi.org/10.1152/ajpheart.00043.2015 (2015).
16. Coughlan, M. T. *et al.* Advanced glycation end products are direct modulators of beta-cell function. *Diabetes* **60**, 2523–2532, https://doi.org/10.2337/db10-1033 (2011).
17. Lo, M. C. *et al.* Nepsilon-(carboxymethyl) lysine-induced mitochondrial fission and mitophagy cause decreased insulin secretion from beta-cells. *American journal of physiology. Endocrinology and metabolism* **309**, E829–839, https://doi.org/10.1152/ajpendo.00151.2015 (2015).

18. Mao, Y. X. *et al*. RAGE-dependent mitochondria pathway: a novel target of silibinin against apoptosis of osteoblastic cells induced by advanced glycation end products. *Cell death & disease* **9**, 674, https://doi.org/10.1038/s41419-018-0718-3 (2018).
19. Gonzales, S., Wang, C., Levene, H., Cheung, H. S. & Huang, C. C. ATP promotes extracellular matrix biosynthesis of intervertebral disc cells. *Cell and tissue research* **359**, 635–642, https://doi.org/10.1007/s00441-014-2042-2 (2015).
20. Tan, K. C. *et al*. Advanced glycation end products and endothelial dysfunction in type 2 diabetes. *Diabetes Care* **25**, 1055–1059 (2002).
21. Hu, Y. *et al*. Mitochondrial Pathway Is Involved in Advanced Glycation End Products-Induced Apoptosis of Rabbit Annulus Fibrosus Cells. *Spine*, https://doi.org/10.1097/brs.0000000000002930 (2018).
22. Guney, A. *et al*. Biomechanical properties of Achilles tendon in diabetic vs. non-diabetic patients. *Exp Clin Endocrinol Diabetes* **123**, 428–432, https://doi.org/10.1055/s-0035-1549889 (2015).
23. James, V. J., Delbridge, L., McLennan, S. V. & Yue, D. K. Use of X-ray diffraction in study of human diabetic and aging collagen. *Diabetes* **40**, 391–394 (1991).
24. Abate, M., Schiavone, C. & Salini, V. Sonographic evaluation of the shoulder in asymptomatic elderly subjects with diabetes. *BMC musculoskeletal disorders* **11**, 278, https://doi.org/10.1186/1471-2474-11-278 (2010).
25. Bedi, A. *et al*. Diabetes mellitus impairs tendon-bone healing after rotator cuff repair. *Journal of shoulder and elbow surgery* **19**, 978–988, https://doi.org/10.1016/j.jse.2009.11.045 (2010).
26. Fox, A. J. *et al*. Diabetes mellitus alters the mechanical properties of the native tendon in an experimental rat model. *Journal of orthopaedic research: official publication of the Orthopaedic Research Society* **29**, 880–885, https://doi.org/10.1002/jor.21327 (2011).
27. de Oliveira, R. R. *et al*. Experimental diabetes induces structural, inflammatory and vascular changes of Achilles tendons. *PloS one* **8**, e74942, https://doi.org/10.1371/journal.pone.0074942 (2013).
28. Wu, Y. F. *et al*. High glucose alters tendon homeostasis through downregulation of the AMPK/Egr1 pathway. *Scientific reports* **7**, 44199, https://doi.org/10.1038/srep44199 (2017).
29. Tsai, W. C. *et al*. High glucose concentration up-regulates the expression of matrix metalloproteinase-9 and -13 in tendon cells. *BMC musculoskeletal disorders* **14**, 255, https://doi.org/10.1186/1471-2474-14-255 (2013).
30. Patel, S. H., Sabbaghi, A. & Carroll, C. C. Streptozotocin-induced diabetes alters transcription of multiple genes necessary for extracellular matrix remodeling in rat patellar tendon. *Connective tissue research*, 1–11, https://doi.org/10.1080/03008207.2018.1470168 (2018).
31. Yang, G., Rothrauff, B. B. & Tuan, R. S. Tendon and ligament regeneration and repair: clinical relevance and developmental paradigm. *Birth defects research. Part C. Embryo today: reviews* **99**, 203–222, https://doi.org/10.1002/bdrc.21041 (2013).
32. Thomopoulos, S., Parks, W. C., Rifkin, D. B. & Derwin, K. A. Mechanisms of tendon injury and repair. *Journal of orthopaedic research: official publication of the Orthopaedic Research Society* **33**, 832–839, https://doi.org/10.1002/jor.22806 (2015).
33. Abate, M. *et al*. Pathogenesis of tendinopathies: inflammation or degeneration? *Arthritis Res Ther* **11**, 235, https://doi.org/10.1186/ar2723 (2009).
34. Ahmed, A. S. Does Diabetes Mellitus Affect Tendon Healing? *Advances in experimental medicine and biology* **920**, 179–184, https://doi.org/10.1007/978-3-319-33943-6_16 (2016).
35. Ahmed, A. S. *et al*. Type 2 diabetes impairs tendon repair after injury in a rat model. *J Appl Physiol* **113**, 1784–1791, https://doi.org/10.1152/japplphysiol.00767.2012 (2012).
36. Abate, M., Schiavone, C., Salini, V. & Andia, I. Occurrence of tendon pathologies in metabolic disorders. *Rheumatology (Oxford)* **52**, 599–608, https://doi.org/10.1093/rheumatology/kes395 (2013).
37. Lui, P. P. Y. Tendinopathy in diabetes mellitus patients-Epidemiology, pathogenesis, and management. *Scand J Med Sci Sports* **27**, 776–787, https://doi.org/10.1111/sms.12824 (2017).
38. Li, G., Xu, J. & Li, Z. Receptor for advanced glycation end products inhibits proliferation in osteoblast through suppression of Wnt, PI3K and ERK signaling. *Biochemical and biophysical research communications* **423**, 684–689, https://doi.org/10.1016/j.bbrc.2012.06.015 (2012).
39. Brand, M. D., Chien, L. F., Ainscow, E. K., Rolfe, D. F. & Porter, R. K. The causes and functions of mitochondrial proton leak. *Biochimica et biophysica acta* **1187**, 132–139, https://doi.org/10.1016/0005-2728(94)90099-x (1994).
40. Zorova, L. D. *et al*. Mitochondrial membrane potential. *Analytical biochemistry* **552**, 50–59, https://doi.org/10.1016/j.ab.2017.07.009 (2018).
41. Killian, M. L. & Thomopoulos, S. Scleraxis is required for the development of a functional tendon enthesis. *Faseb j* **30**, 301–311, https://doi.org/10.1096/fj.14-258236 (2016).
42. Owen, W. F. Jr. *et al*. Beta 2-microglobulin modified with advanced glycation end products modulates collagen synthesis by human fibroblasts. *Kidney international* **53**, 1365–1373, https://doi.org/10.1046/j.1523-1755.1998.00882.x (1998).
43. Merkel, J. R., DiPaolo, B. R., Hallock, G. G. & Rice, D. C. Type I and type III collagen content of healing wounds in fetal and adult rats. *Proceedings of the Society for Experimental Biology and Medicine. Society for Experimental Biology and Medicine (New York, N.Y.)* **187**, 493–497 (1988).
44. Hurme, T., Kalimo, H., Sandberg, M., Lehto, M. & Vuorio, E. Localization of type I and III collagen and fibronectin production in injured gastrocnemius muscle. *Laboratory investigation; a journal of technical methods and pathology* **64**, 76–84 (1991).
45. Nah, S. S. *et al*. Advanced glycation end products increases matrix metalloproteinase-1, −3, and −13, and TNF-alpha in human osteoarthritic chondrocytes. *FEBS letters* **581**, 1928–1932, https://doi.org/10.1016/j.febslet.2007.03.090 (2007).
46. Menshikova, E. V. *et al*. Effects of exercise on mitochondrial content and function in aging human skeletal muscle. *The journals of gerontology. Series A, Biological sciences and medical sciences* **61**, 534–540 (2006).
47. Shigenaga, M. K., Hagen, T. M. & Ames, B. N. Oxidative damage and mitochondrial decay in aging. *Proceedings of the National Academy of Sciences of the United States of America* **91**, 10771–10778 (1994).
48. Kim, M. M. *et al*. Mitochondrial DNA quantity increases with histopathologic grade in premalignant and malignant head and neck lesions. *Clinical cancer research: an official journal of the American Association for Cancer Research* **10**, 8512–8515, https://doi.org/10.1158/1078-0432.ccr-04-0734 (2004).
49. Lee, H. C., Yin, P. H., Lu, C. Y., Chi, C. W. & Wei, Y. H. Increase of mitochondria and mitochondrial DNA in response to oxidative stress in human cells. *The Biochemical journal* **348**(Pt 2), 425–432 (2000).
50. Pun, P. B. & Murphy, M. P. Pathological significance of mitochondrial glycation. *International journal of cell biology* **2012**, 843505, https://doi.org/10.1155/2012/843505 (2012).
51. Cline, S. D. Mitochondrial DNA damage and its consequences for mitochondrial gene expression. *Biochimica et biophysica acta* **1819**, 979–991, https://doi.org/10.1016/j.bbagrm.2012.06.002 (2012).
52. Ott, M., Gogvadze, V., Orrenius, S. & Zhivotovsky, B. Mitochondria, oxidative stress and cell death. *Apoptosis: an international journal on programmed cell death* **12**, 913–922, https://doi.org/10.1007/s10495-007-0756-2 (2007).
53. Sifuentes-Franco, S., Pacheco-Moises, F. P., Rodriguez-Carrizalez, A. D. & Miranda-Diaz, A. G. The Role of Oxidative Stress, Mitochondrial Function, and Autophagy in Diabetic Polyneuropathy. *Journal of diabetes research* **2017**, 1673081, https://doi.org/10.1155/2017/1673081 (2017).
54. Hildeman, D. A. *et al*. Control of Bcl-2 expression by reactive oxygen species. *Proceedings of the National Academy of Sciences of the United States of America* **100**, 15035–15040, https://doi.org/10.1073/pnas.1936213100 (2003).
55. Zorov, D. B., Juhaszova, M. & Sollott, S. J. Mitochondrial reactive oxygen species (ROS) and ROS-induced ROS release. *Physiol Rev* **94**, 909–950, https://doi.org/10.1152/physrev.00026.2013 (2014).

56. Jiang, X. & Wang, X. Cytochrome C-mediated apoptosis. *Annu Rev Biochem* **73**, 87–106, https://doi.org/10.1146/annurev.biochem.73.011303.073706 (2004).
57. Wang, Z. *et al*. Effect of advanced glycosylation end products on apoptosis in human adipose tissue-derived stem cells *in vitro*. *Cell & bioscience* **5**, 3, https://doi.org/10.1186/2045-3701-5-3 (2015).
58. Zheng, F. *et al*. Transient overexpression of TGFBR3 induces apoptosis in human nasopharyngeal carcinoma CNE-2Z cells. *Bioscience reports* **33**, e00029, https://doi.org/10.1042/bsr20120047 (2013).
59. Valencia, J. V. *et al*. Advanced glycation end product ligands for the receptor for advanced glycation end products: biochemical characterization and formation kinetics. *Analytical biochemistry* **324**, 68–78 (2004).
60. Westwood, M. E. & Thornalley, P. J. Molecular characteristics of methylglyoxal-modified bovine and human serum albumins. Comparison with glucose-derived advanced glycation endproduct-modified serum albumins. *Journal of protein chemistry* **14**, 359–372 (1995).
61. Verzijl, N. *et al*. Age-related accumulation of Maillard reaction products in human articular cartilage collagen. *The Biochemical journal* **350**(Pt 2), 381–387 (2000).
62. Monnier, V. M., Kohn, R. R. & Cerami, A. Accelerated age-related browning of human collagen in diabetes mellitus. *Proceedings of the National Academy of Sciences of the United States of America* **81**, 583–587 (1984).
63. Council, N. R. *Guide for the Care and Use of Laboratory Animals*. 8th edn, (The National Academies Press, 2011).
64. Salic, A. & Mitchison, T. J. A chemical method for fast and sensitive detection of DNA synthesis *in vivo*. *Proceedings of the National Academy of Sciences of the United States of America* **105**, 2415–2420, https://doi.org/10.1073/pnas.0712168105 (2008).
65. Li, B. *et al*. Droplet digital PCR shows the D-Loop to be an error prone locus for mitochondrial DNA copy number determination. *Scientific reports* **8**, 11392, https://doi.org/10.1038/s41598-018-29621-1 (2018).
66. Memon, A. A. *et al*. Quantification of mitochondrial DNA copy number in suspected cancer patients by a well optimized ddPCR method. *Biomolecular detection and quantification* **13**, 32–39, https://doi.org/10.1016/j.bdq.2017.08.001 (2017).
67. Patel, S. H. *et al*. Impact of acetaminophen consumption and resistance exercise on extracellular matrix gene expression in human skeletal muscle. *Am J Physiol Regul Integr Comp Physiol* **313**, R44–r50, https://doi.org/10.1152/ajpregu.00019.2017 (2017).
68. Kawase, M. *et al*. Exacerbation of delayed cell injury after transient global ischemia in mutant mice with CuZn superoxide dismutase deficiency. *Stroke* **30**, 1962–1968 (1999).
69. Nazarewicz, R. R., Bikineyeva, A. & Dikalov, S. I. Rapid and specific measurements of superoxide using fluorescence spectroscopy. *Journal of biomolecular screening* **18**, 498–503, https://doi.org/10.1177/1087057112468765 (2013).
70. Hildeman, D. A. *et al*. Reactive oxygen species regulate activation-induced T cell apoptosis. *Immunity* **10**, 735–744 (1999).

Acknowledgements

This work was supported by NIH pre-doctoral fellowship F31-AR073647 (SHP) and Purdue University Research Initiative Funds (CCC). The authors would like to acknowledge Christopher Kargl and Zachary Hettinger for technical laboratory assistance.

Author Contributions

S.H.P. and C.C.C. conceived and designed the study. S.H.P., F.Y., S.K.S., R.F., A.S. and C.C.C. performed data collection and analysis. S.H.P., F.Y., S.K.S., R.F., J.R.C., J.H.S., S.K., A.S. and C.C.C. interpreted data and provided expert advice. S.H.P. and C.C.C. drafted the manuscript. All authors edited, revised, read, and approved the final submitted manuscript.

Additional Information

Supplementary information accompanies this paper at https://doi.org/10.1038/s41598-019-49062-8.

Competing Interests: The authors declare no competing interests.

Publisher's note: Springer Nature remains neutral with regard to jurisdictional claims in published maps and institutional affiliations.